Finite volume method and high accuracy 2D code for protoplanetary disks

Tarik Chakkour

Finite volume method and high accuracy 2D code for protoplanetary disks

Tarik Chakkour

Univ. Bretagne-Sud, UMR 6205, LMBA, F-56000 Vannes, France

February 4, 2018

Abstract. We investigate in this paper a hydrodynamical code in order to simulate the flow of gas and solid particles in protoplanetary disks. This code is devoted to explore planetary formation at the decoupling stage when the gas and solid phases are competing with one another. In this work our goal is to study the full time evolution of gas and particles around the star and is to characterize the Rossby wave instability in 2D.

Keywords: Hydrodynamics; protoplanetary disks; finite volume scheme.

1 Introduction

Planetesimal formation is obviously an important process in the realm of solar-type stars, as we know from the Solar System that such stars can form planets. There is also ample evidence from the recent observations of extrasolar planets surrounding solar-type stars. In paper [7] we deals with the detection of two of the most eccentric known planets. Nevertheless, the first planets detected outside the Solar System were orbiting pulsars, indicating that planet (and therefore planetesimal) formation is also possible around massive stars. Observations indicate in [9] that at least one more planet may be present in the system. It has been speculated and was recently observed in at least one case that fall-back material can form a disk surrounding the remnant star after a supernova explosion. The author investigates in [8] fallback disks around young neutron stars. This lends support to the idea that planetesimal formation might not only accompany star formation but might also proceed under a variety of conditions, possibly even around dying stars.

Planet formation is believed to occur in the disks of gas and dust that surround young solar-type stars. Most stars, however, form in multiple systems, where the presence of a close companion could affect the structure of the disk and perhaps interfere with planet formation. The author investigates in [1] the gravitational interaction of a generally eccentric binary star system with circumbinary and circumstellar gaseous disks. It has been difficult to investigate this because of the resolution needed. Here we report interferometric observations (at a wavelength of 7 mm) of the core of the star-forming region L1551 (line observations of the pre-stellar core with the Nobeyama 45 m telescope and Millimter Array). We have achieved a linear resolution of seven astronomical units (less than the diameter of Jupiter's orbit). The core of L1551 contains two distinct disks, with a separation of 45 AU; these appear to be associated with a binary system. Both disks are spatially resolved, with semi-major axes of about 10 AU, which is about a factor of ten smaller than disks around isolated stars. The author review in [2] the ground-based and Infrared Space Obser atory (ISO) data on the small-grain components of the inner disk regions. The disk masses are of order 0.05 solar masses, which could be enough to form planetary systems like our own.

Our study was motivated by authors of paper [6] (2003), who investigated the evolution of gravitationally unstable protoplanetary gaseous disks using three dimensional smoothed particle hydrodynamics (SPH) simulations with unprecedented resolution. They have done simulations with codes that solve the hydrodynamical equations on a fixed grid show that slightly perturbed disks form strong spiral arms

and overdensities. Here we report on the results of new 2D simulations of unstable protoplanetary disk which is extended from 5 to 10 AU initially and is in nearly keplerian rotation around a solar mass star represented by a point mass.

Numerical methods are essential for the study of a very wide range of problems in astrophysical fluid dynamics. As such, the development of more accurate and more capable algorithms, that is important for progress in the field. This paper describes a new code for planetary formation. This code simulates the flow of gas and solid particles in protoplanetary disks. It has been designed to be easily extensible for use with static and adaptive mesh refinement. It combines Godunov method for evaluating the radial flux and the azimuthal flux which is approached by a cell-centred scheme.

In this paper, we are interested in the formation of 2D vortices and in their long-term evolution. The paper is structured as follows. In section 3 we briefly describe the Euler and continuity equations for the motion of gas then take the explicit form. Details of the modeling, including the full discretization and the numerical method is found in section 4 that is shared in three subsections. We describe in first subsection 4.1 the 2D cylindrical domain where we integrate these equations over it. The continuous spatial coordinates (r, θ) are discretized into a finite size (n_r, n_θ) in each direction, respectively. It is followed by the initial conditions presented in second subsection 4.2. The principle of finite volume schemes and their ability to conserve the integral of the transported properties will be introduced in third subsection 4.3. Next, a high accuracy hydrodynamical code has been developed and tested in section 5 in order to simulate the evolution of a protoplanetary disk. We check particularly the steady state. The Rossby wave instability is found in final section to proceed in 2D. Their formation and stability is a complex problem and still a matter of debate.

2 Modeling a Keplerian flow

In the present work we first investigate the planetesimal formation in a compressible Keplerian disk. We then perform simulations intended to study the dynamics in the presence of two-phase. We discuss here the technical details of the modeling the equilibrium over the Keplerian disc. This modeling is presented in Figure 1. The numerical simulation of two-phase dilute flow (droplet-gas mixture) is the object of great attention from researchers. This interest is due to a lot of applications. We model the flow by a coupled system of Euler equations. This allows to establish practical results, as well as the the study of numerical scheme. Two-phase flow is divided into two categories. The first one is to separate flow phase, which is the type of flow that occurs when the debit of gas and liquid are low. The second one is dispersed flow, for example the formation of air bubbles during the agitation of a water bottle.

We define a control volume by a delimited domain of each cell in order to follow the evolution of average of quantities. This Eulerian approach allows to optimize the computation time by taking into account the fact that the dispersed phase affects the gas phase. Consequently, for modeling two phases in control volume, each these two volumes are separated by an interface. It is through this interface that there has been an interaction between two pahses.

Assuming that the disk is at hydrostatic equilibrium along the axis z, which occurs if the movements along this axis are subsonic. The equilibrium hydrostatic equation is given by:

$$\overrightarrow{gradP} = -\rho.\overrightarrow{grad\Phi}, \tag{1}$$

where Φ is the gravitational potential. If $r \in [r_{\min} r_{\max}]$, then the effect of the gravitational field component coming from the mass of disk (self-gravitation) is neglected. This potetiel Φ is then written as: $\Phi = -\frac{GM}{D}$, where $D = \sqrt{r^2 + z^2}$ is the distance from the considered point of system center, which gives over the axis z, the following equality:

$$\frac{1}{\rho}\frac{\partial P}{\partial z} = \frac{\partial}{\partial z}\frac{GM}{(r^2 + z^2)^{\frac{1}{2}}}. \tag{2}$$

Assuming that the orbits are circular and obey Kepler's laws. If the disk is thin $z^2 \ll r^2$, we get:

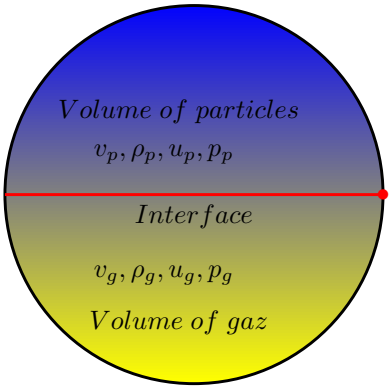

Figure 1: Modelization of two-phase flow.

$$\begin{aligned} \frac{1}{\rho}\frac{\partial P}{\partial z} &= \frac{\partial}{\partial z}\frac{GM}{r}\left(1-\frac{z^2}{2r^2}\right), \\ &= -\frac{GM}{r^3}z, \\ &= -\Omega^2 z, \end{aligned} \tag{3}$$

where Ω means the angular velocity which is given by:

$$\Omega = \sqrt{\frac{GM}{r^3}}. \tag{4}$$

The equilibrium over the Keplerian disc is written as:

$$\frac{v^2}{r} = \frac{GM}{r^2} \tag{5}$$

The solid particles perform quasi-Keplerian orbits in the plane of the disc, whereas they perform oscillations around the middle equatorial plane in a perpendicular direction at the plane of the disk.

3 Euler equations

The Euler equation can express the mass, momentum and energy conservation in local form as a function of density of the radial velocity u, of the azimuthal velocity v, of pressure p and of the internal energy E. The total energy e is the sum of the kinetic and internal energy. Let us consider initially an ideal fluid. For polytropic gaz law, with $\gamma > 1$, energy, pressure and temperature are given by the following relations:

$$\begin{cases} e = \frac{1}{2}(u^2+v^2) + E, \\ p = (\gamma-1)\rho E, \\ T = \frac{\mu}{kb}\frac{p}{\rho}. \end{cases} \tag{6}$$

It is useful to define vector of the conserved variables w, with components in cylindrical coordinates

$$w = \begin{pmatrix} \rho \\ \rho u \\ \rho v \\ \rho e \end{pmatrix}.$$

Defining vector w as an application:

$$w : \left| \begin{array}{ccc} [0,\infty[\times \mathbf{R} \times [0,2\pi] & \longrightarrow & \mathbf{R^3} \\ (t,r,\theta) & \longmapsto & w(t,r,\theta). \end{array} \right.$$

The conservation laws can now be written in a compact form (in cylindrical coordinates),

$$\frac{\partial w}{\partial t} + \frac{1}{r}\frac{\partial r F(w)}{\partial r} + \frac{1}{r}\frac{\partial G(w)}{\partial r} = Q(r,w), \tag{7}$$

where F, G are vectors of fluxes in the $\vec{e_r}$ and $\vec{e_\theta}$ directions, respectively, with components

$$F(w) = \begin{pmatrix} \rho u \\ \rho u^2 + p \\ \rho uv \\ (\rho e + p)u \end{pmatrix},$$

and

$$G(w) = \begin{pmatrix} \rho v \\ \rho uv \\ \rho v^2 + p \\ (\rho e + p)v \end{pmatrix},$$

and where the source term is defined as:

$$Q(w) = \begin{pmatrix} 0 \\ \dfrac{\rho v^2}{r} - \rho\dfrac{GM}{r^2} + \dfrac{p}{r} + F_r \\ -\dfrac{\rho uv}{r} + F_\theta \\ -\rho u\dfrac{GM}{r^2} \end{pmatrix}.$$

Denoting by F_θ and F_r the friction forces exerted by the gas on the particles per volume unit given by:

$$\begin{cases} F_r = \frac{3}{2}\frac{\rho_g . c.l}{\rho_{mat} r_d^2}\rho_d(u_d - u_g), \\ F_\theta = \frac{3}{2}\frac{\rho_g . c.l}{\rho_{mat} r_d^2}\rho_d(v_d - v_g). \end{cases}$$

If there is only gaz, the friction forces are nuls. We have:

$$\begin{cases} \rho_g : \text{ gas density} \\ \rho_d : \text{ particle density} \\ c : \text{ speed of sound} \\ \rho_{mat} : \text{ constant fixed at } 3g/cm^3 \\ u_g, v_g : \text{ vertical and azimuthal velocities for gas} \\ u_d, v_d : \text{ vertical and azimuthal velocities for particle} \\ l : \text{ angular momentum} \end{cases}$$

The angular momentum l for the solid particles satisfies the following differential equation:

$$\frac{\partial l}{\partial t} + \frac{1}{r}\frac{\partial r l u}{\partial r} + \frac{1}{r}\frac{\partial l v}{\partial \theta} = 0. \tag{8}$$

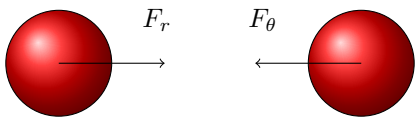

Figure 2: Action and reaction theory for frictional forces.

4 Numerical scheme

4.1 Computational domain

The computational domain can be subdivided into a finite number of cells. These cells cover entirely the computational domain and provide a good geometrical approximation of the flow. The flow of gas and particles is studied in a ring around the star with inner and outer radii denoted by $r_{\text{in}} = 5\text{AU}$ and $r_{\text{out}} = 10\text{AU}$, respectively. The physical domain is illustrated in Figure 4. For the numerical description, the variables are discretized on an annular grid divided into n_r and n_θ pieces, respectively for the radial and azimuthal directions. The grid is regularly spaced with:

$$\begin{cases} \Delta r = \frac{r_{\text{out}} - r_{\text{in}}}{n_r}, \\ \Delta\theta = \frac{2\pi}{n_\theta}. \end{cases} \tag{9}$$

The cells are labeled with the index i in the radial direction and with the index j in the azimuthal direction as follows:

$$\begin{cases} r_i = r_{int} + (i - \frac{1}{2})\Delta r, \\ \theta_j = (j - \frac{1}{2})\Delta\theta. \end{cases} \tag{10}$$

The configuration of the cell is illustrated in Figure 5. In the radial direction the boundaries of the cell are given by $r_i + \frac{\Delta r}{2}$ and $r_i - \frac{\Delta r}{2}$, while in the azimuthal direction they are given by $\theta_j + \frac{\Delta\theta}{2}$ and $\theta_j - \frac{\Delta\theta}{2}$, respectively. The average values of the quantities are stored for each cell with using finite volume method.

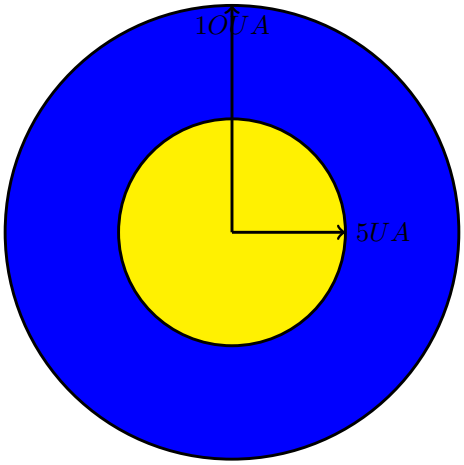

Figure 3: Computational domain.

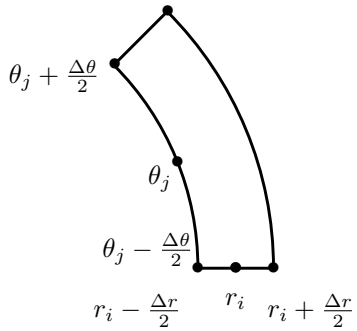

Figure 4: Cylindrical cell

Our goal is to define ghost cells at every point in the computational domain. The use of ghost cells (actually ghost nodes in our finite volume framework) is to keep the scheme robust and easy to program with simple extensions to multidimensions and multilevel time integration. To produce ghost cells that satisfy the appropriate boundary conditions for the Euler equations, we present them in Figure 6 for each cell $\left[r_{i-1/2}, r_{i+1/2}\right] \times \left[\theta_{j-1/2}, \theta_{j+1/2}\right]$. The pincipal geometrical data to know is the surface $S_{i,j}$ defined by the angular variation:

$$S_{i,j} = r_i \Delta\theta \Delta r. \tag{11}$$

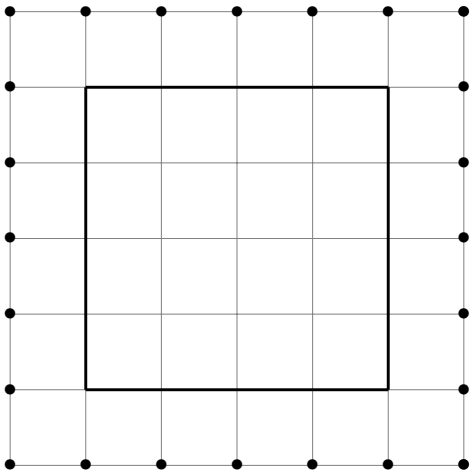

Figure 5: Ghost cells.

The surface vectors allow to determine the radial and the azimuthal flux, which are related to each of the faces of the considered cell. We express the lengths of each facet presented in Figure 7 as follows:

$$\begin{cases} \vec{l}_{i-1/2,j} = -r_{i-1/2}\Delta\theta\vec{e_r}, \\ \vec{l}_{i+1/2,j} = -r_{i+1/2}\Delta\theta\vec{e_r}, \\ \vec{l'}_{i,j-1/2} = -\Delta r\vec{e_\theta}, \\ \vec{l'}_{i,j+1/2} = \Delta r\vec{e_\theta}. \end{cases} \tag{12}$$

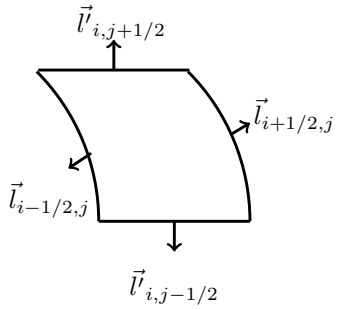

Figure 6: The surface vectors.

4.2 Initial conditions

The purpose of this subsection is to provide initial conditions that is an essential part of conceptualizing and modeling the flow of gas and solid particles used for protoplanetary disks. The specification of appropriate initial conditions is important in this topic because is also the part most subject to serious error by hydrologists. We explain here the concept of initial conditions and we discuss some common pitfalls in the model. The initial conditions are chosen within the framework of the disk model introduced by Hayashi et al. in paper [3] (1985). The gas is assumed to be a mixture of hydrogen molecules and helium with a small amount of heavy elements. The initial conditions are given as follows:

$$\begin{cases} \rho_{init} = \rho_0(\frac{r}{r_0})^{-3/2}, \\ T_{init} = T_0(\frac{r}{r_0})^{-1/2}, \\ p_{init} = p_0(\frac{r}{r_0})^{-2}, \\ u_{init} = 0, \\ v_{init} = \sqrt{\frac{GM}{r_0}(r_0/r) - 2\frac{p}{\rho}}, \end{cases} \tag{13}$$

where

$$\begin{cases} \rho_0 = 1.4.10^{-6} Kg.m^{-3}, \\ T_0 = 280K, \\ p_0 = 1.42Pa. \end{cases} \tag{14}$$

4.3 Numerical method

The conservation laws defined by equation in (7) can be written in following form:

$$\partial_t w + \nabla . f(w) = Q(w). \tag{15}$$

The finite volume method is a method for representing and evaluating partial differential equations in the form of algebraic equations. The values are calculated at discrete places on a meshed geometry. In this computational fluid dynamics package, the average of the conserved variables is stored alongside the two radial and azimuth meshes defining a control volume. In the finite volume method, volume integrals in a partial differential equation that contain a divergence term (see equation (15)) are converted to surface integrals, using the divergence theorem. These terms are then evaluated as fluxes at the surfaces of each finite volume. Because the flux entering a given volume is identical to that leaving the adjacent volume, these methods are conservative. Another advantage of the finite volume method is that it is easily formulated to allow for unstructured meshes. Discretizations based on the integral, rather than the differential, form of equation (7) have numerous advantages for flows that contain shocks and discontinuities (LeVeque 2002). Integration of equation (15) over the volume of a grid cell $\Omega_{i,j}$ delimited by the surface $S_{i,j}$ gives:

$$\int_{\Omega_{i,j}} \left(\frac{\partial w}{\partial t} + \nabla . f(w) \right) d\Omega = \int_{\Omega_{i,j}} Q d\Omega. \tag{16}$$

Assuming that $w_{i,j}$ is the average value on each control volume $\Omega_{i,j}$, and using Gauss's theorem, the equation is written:

$$\frac{\partial w}{\partial t}\Omega_{i,j} + \int_{\partial\Omega_{i,j}} f(w) d\Omega = \int_{\Omega_{i,j}} Q d\Omega. \tag{17}$$

The conserved variable w, and the source terms Q are averaged over control volume $\Omega_{i,j}$:

$$\begin{cases} w_{i,j} = \dfrac{1}{\Omega_{i,j}} \displaystyle\int_{\Omega_{i,j}} w d\Omega, \\ Q_{i,j} = \dfrac{1}{\Omega_{i,j}} \displaystyle\int_{\Omega_{i,j}} Q d\Omega. \end{cases} \tag{18}$$

The fluxes are computed on each of the faces, the radial flux F according to the components l, and the azimuthal flux G according to the components l'. The discrete-time linear systems is written in following form:

$$\frac{\partial w_{i,j}\Omega_{i,j}}{\partial t} + \sum_{l} \vec{F}.\vec{S} + \sum_{l'} \vec{G}.\vec{S} = Q_{i,j}\Omega_{i,j}. \tag{19}$$

Time is discretized into N uniform steps between the initial value t_0 and the final stopping time t_f. Following the usual convention $t^{n+1} - t^n = \Delta t$. The variation of quantity $w_{i,j}$ can be determined at each time step Δt:

$$\Delta w_{i,j} = \Delta t \left(Q_{i,j} - \frac{\sum_{l} \vec{F}.\vec{S} + \sum_{l'} \vec{G}.\vec{S}}{S_{i,j}} \right). \tag{20}$$

An other discretization form of equation (20) is given by the following equality:

$$w_{i,j}^{n+1} = w_{i,j}^{n} + \Delta t \left(Q_{i,j}^{n} - \frac{F_{i+1/2,j}^{n} l_{i+1/2,j} - F_{i-1/2,j}^{n} l_{i-1/2,j} + G_{i,j+1/2}^{n} l'_{i,j+1/2} - G_{i,j-1/2}^{n} l'_{i,j-1/2}}{S_{i,j}^{n}} \right). \tag{21}$$

The equation defined by (7) is resolved by a splitting extrapolation method, we are able to present the general result equivalent to (7), i.e.

$$\begin{cases} \frac{\partial w}{\partial t} + \frac{1}{r}\frac{\partial rF(w)}{\partial r} = Q(r,w), \\ \frac{\partial w}{\partial t} + \frac{1}{r}\frac{\partial G(w)}{\partial r} = Q(r,w). \end{cases} \tag{22}$$

The azimuthal flux G is approached by a cell-centred scheme. In order to preserve the hyperbolic character and to balance the bidimensional numerical scheme, we keep the same the undimensional radial flux F.

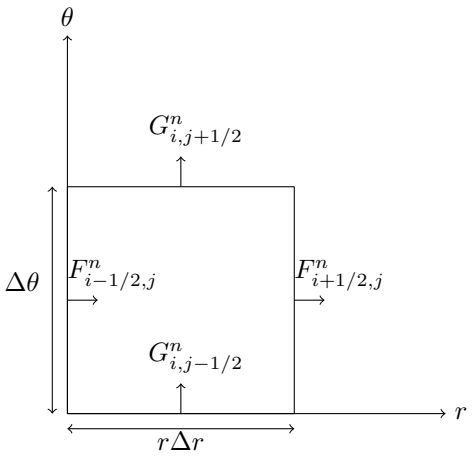

Figure 7: Discretization by the finite volume method over a cylindrical domain.

Assuming that G is twice-derivable-function over interval $\left[r_i, \theta_j - \frac{\Delta\theta}{2}\right] \times \left[r_i, \theta_j + \frac{\Delta\theta}{2}\right]$, function G is Taylor-Young expanded in $(r_i, \theta_j + \frac{\Delta\theta}{2})$ until the order 2 to obtain:

$$G\left(r_i, \theta_j + \frac{\Delta\theta}{2}\right) = G(r_i, \theta_j) + \frac{\Delta\theta}{2}\left(\frac{\partial G}{\partial\theta}\right)_{r_i,\theta_j} + \frac{(\Delta\theta)^2}{8}\left(\frac{\partial G}{\partial\theta}\right)_{r_i,\theta_j} + \frac{(\Delta\theta)^2}{4}\varepsilon_1(\Delta\theta), \tag{23}$$

and function G is Taylor-Young expanded in $(r_i, \theta_j - \frac{\Delta\theta}{2})$ until the order 2 to obtain:

$$G\left(r_i, \theta_j - \frac{\Delta\theta}{2}\right) = G(r_i, \theta_j) - \frac{\Delta\theta}{2}\left(\frac{\partial G}{\partial \theta}\right)_{r_i,\theta_j} + \frac{(\Delta\theta)^2}{8}\left(\frac{\partial G}{\partial \theta}\right)_{r_i,\theta_j} + \frac{(\Delta\theta)^2}{4}\varepsilon_2(\Delta\theta), \tag{24}$$

where all applications ε_i, with $i \in \{1, 2\}$, converge to 0 when $\Delta\theta$ goes to 0. Subtracting equation (23) from equation (24), we get:

$$\frac{G_{i,j+\frac{1}{2}} - G_{i,j-\frac{1}{2}}}{\Delta\theta} = \left(\frac{\partial G}{\partial \theta}\right)_{(r_i,\theta_j)} + \mathcal{O}(\Delta\theta^2). \tag{25}$$

The second-order discretization for the flux G is defined from the upstream approximation at the interface $(r_i, \theta_{j+\frac{1}{2}})$ and the downstream approximation at the interface $(r_i, \theta_{j-\frac{1}{2}})$ as follows:

$$G_{i,j+\frac{1}{2}} = \begin{pmatrix} \rho_{i,j+\frac{1}{2}} v_{i,j+\frac{1}{2}} \\ \rho_{i,j+\frac{1}{2}} u_{i,j+\frac{1}{2}} v_{i,j+\frac{1}{2}} \\ \rho_{i,j+\frac{1}{2}} v^2_{i,j+\frac{1}{2}} + p_{i,j+\frac{1}{2}} \\ (\rho_{i,j+\frac{1}{2}} e_{i,j+\frac{1}{2}} + p_{i,j+\frac{1}{2}}) v_{i,j+\frac{1}{2}} \end{pmatrix}.$$

The Courant-Friedrichs-Lewy (CFL) condition is a necessary condition for convergence while solving the partial differential equation defined by (7) numerically by the finite volume method. It arises in the numerical analysis of explicit time integration schemes, when these are used for the numerical solution. For gas the time step Δt is given as follows:

$$\Delta t = C_{\text{CFL}} \min(\Delta_{i,j}). \tag{26}$$

If the cells are too small compared with the time step, numerical smearing may occur leading to instability and in some cases divergence. If time step Δt depends on chosen cell $\Omega_{i,j}$, then it is given by:

$$\Delta t = C_{\text{CFL}} \min\left(\frac{\Delta r}{c^{r,n}_{i,j}}, \frac{\Delta\theta}{c^{\theta,n}_{i,j}}\right), \tag{27}$$

where $c^{r,n}_{i,j}$ and $c^{\theta,n}_{i,j}$ are respectively the speed of propagation inside the cell in the radial and azimuthal directions. Since the rotation of the gas around the sun must be taken into account, this velocity is the sum of two velocities. The first one is the speed of sound and the second one is the speed of the wave in propagation. In the one-dimensional case, $c_{i,j}$ means the speed of sound. The coefficient CFL is chosen from such so that the condition of numerical stability is verified. The flux depend necessarily on coefficient CFL, for the method of 1^{st} order, we take in practice $C_{\text{CFL}} \simeq 0.9$. In ths numerical code, we use the following time step Δt defined by:

$$\Delta t = \min\left(\Delta t_0, \frac{S_{i,j}}{v\Delta r + u r_{i+1/2}\Delta\theta + \sqrt{\frac{\gamma p}{e}(\Delta r^2 + \Delta\theta {r_{i+1/2}}^2)}}\right). \tag{28}$$

5 Testing the code accuracy in two-dimensional space

We test in this section the capacity of the code to keep a gas disk in steady rotation around the star. We precise the duration that the code satisfy the initial steady state solution for the gas. The steady state solution of a gas disk flowing around a central star is will given in simulations, with inner and outer boundaries chosen at 5 and 10 AU, respectively. Simulations are performed over 1000 years and for two-dimensional space. A reasonable grid resolution are 100 cells in the radial direction and the same number of cells in the azimuthal direction.
Now, we check whether the code has the required accuracy to compute the stationary solutions that remain uniform over time. The 2D evolution of the density ρ is presented in Figures 9, 10, 11 and 12. First Figure 9 shows that there is no fluctuations with a scale of approximation 10^{-7} of density ρ. However on a smaller scale than 10^{-7}, the disturbances presented in Figures 10, 11 and 12 begin to appear on the disc.

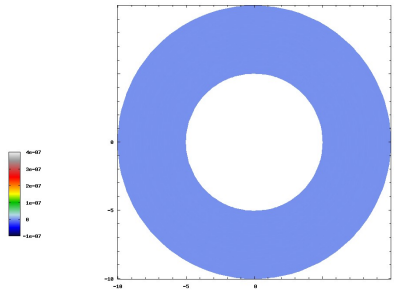

Figure 8: Disk at initial time, with approximation 10^{-7}.

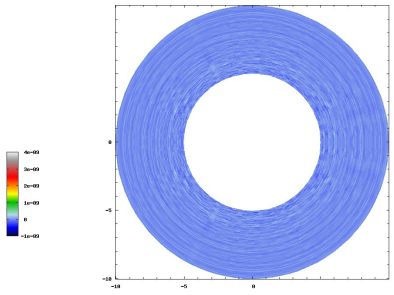

Figure 9: Disk at initial time, with approximation 10^{-10}.

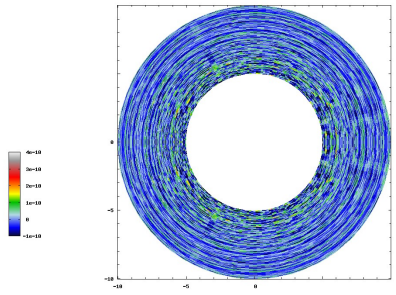

Figure 10: Disk after 500 years, with approximation 10^{-10}.

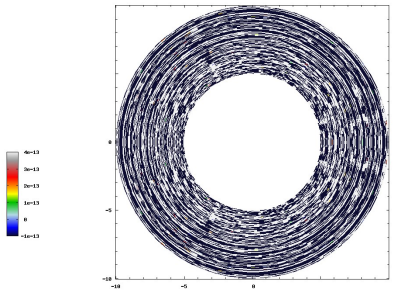

Figure 11: Disk after 1000 years, with approximation 10^{-14}.

6 Stability and long-term evolution

The stability of Rossby waves has been discussed by Lovelace et al. (1999) and Li et al. (2000, 2001) in the evolution of protoplanetary disks. The authors reconsider in [5] the question of the stability of non-magnetized Keplerian disks. In particular, they find a linear instability of non-axisymmetric perturbations for conditions where the disk quantities, such as surface density and entropy have steep radial gradients. The authors study in [4] the nonlinear evolution of the Rossby wave instability in thin disks using global 2D hydrodynamic simulations. Although the result that Rossby waves may be unstable is perhaps surprising from a meteorological viewpoint, it is less remarkable when viewed in the light of vave interaction theory. This instability is primarily responsible for tho loss of predictability observed in numerical atmospheric models, i.e. the divergence observed between the properties of two time integrations with slightly different initial conditions.

We try to produce one of the linear stability, that why we use Gaussian bump. Figures 13, 14, 15 and 16 show that different evolutions of the density ρ in a Rossby-unstable disk. We present in Figure 13, the initial state of Gaussian bump distributed on disk. Inside the vortex, the density field is found to have a Gaussian profile like the background-disk state. The vortex survived more than 3 rotations and its structures were quasi-steady with only two days time-evolution associated with the numerical diffusion.

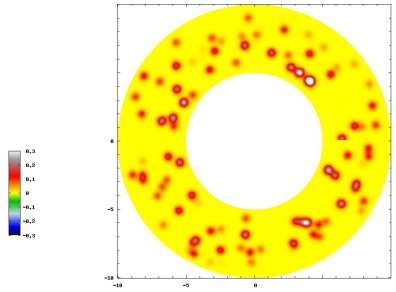

Figure 12: Disk at initial time.

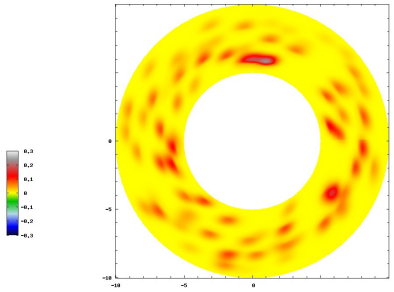

Figure 13: Disk after 10 years.

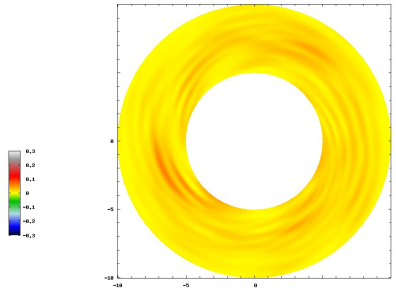

Figure 14: Disk after 15 years.

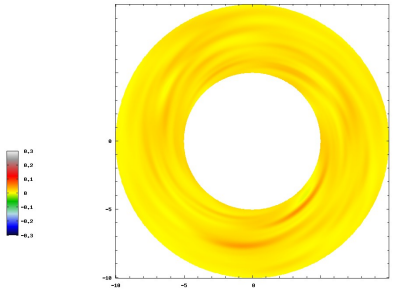

Figure 15: Disk after 25 years.

References

[1] P. Artymowicz and S. H. Lubow. Dynamics of binary-disk interaction. 1: Resonances and disk gap sizes. *apj*, 421:651–667, February 1994.

[2] Carol A Grady, Michael L Sitko, Ray W Russell, David K Lynch, Martha S Hanner, Mario R Perez, Karen S Bjorkman, and Dolf De Winter. Infalling planetesimals in pre-main sequence stellar systems. *Protostars and planets IV*, pages 613–638, 2000.

[3] Ch Hayashi, K Nakazawa, and Y Nakagawa. Formation of the solar system. In *Protostars and planets II*, pages 1100–1153, 1985.

[4] H Li, SA Colgate, B Wendroff, and R Liska. Rossby wave instability of thin accretion disks. iii. nonlinear simulations. *The Astrophysical Journal*, 551(2):874, 2001.

[5] RVE Lovelace, H Li, SA Colgate, and AF Nelson. Rossby wave instability of keplerian accretion disks. *The Astrophysical Journal*, 513(2):805, 1999.

[6] Lucio Mayer, Thomas Quinn, James Wadsley, and Joachim Stadel. Forming giant planets via fragmentation of protoplanetary disks. *arXiv preprint astro-ph/0301088*, 2003.

[7] S Udry, D Fischer, and D Queloz. Protostars and planets v. *Reipurth, D. Jewitt, K. Keil, eds*, pages 685–699, 2007.

[8] Zhongxiang Wang, Deepto Chakrabarty, and David L Kaplan. A debris disk around an isolated young neutron star. *Nature*, 440(7085):772–775, 2006.

[9] Aleksander Wolszczan and Dail A Frail. A planetary system around the millisecond pulsar psr1257+ 12. *Nature*, 355(6356):145–147, 1992.